Jalilvand et al., *BioImpacts.* 2025;15:30300
doi: 10.34172/bi.30300
https://bi.tbzmed.ac.ir/

Fabrication and characterization of nanocomposite scaffold containing zinc-doped mesoporous bioglass: Evaluation of the antioxidant properties, hemocompatibility and proliferation of apical papilla stem cells

Morteza Jalilvand[1], Elham Khoshbin[1], Zahra Barabadi[2], Hamed Karkehabadi[1], Esmaeel Sharifi[2*]

[1]Department of Endodontics, School of Dentistry, Hamadan University of Medical Sciences, Hamadan, Iran
[2]Department of Tissue Engineering, School of Advanced Technologies in Medicine, Hamadan University of Medical Sciences, Hamadan, Iran

Article Info

Article Type:
Original Article

Article History:
Received: 30 Jan. 2024
Revised: 19 Mar. 2024
Accepted: 21 Apr. 2024
ePublished: 28 Oct. 2024

Keywords:
Mesoporous bioactive glass
Zinc
Dental tissue engineering
Alginate
Chitosan

Abstract

Introduction: Nanocomposite scaffolds comprising mesoporous bioactive glass (MBG) were able to increase the viability, proliferation, and growth of stem cells in vitro, rendering them promising candidates for dental root tissue regeneration.

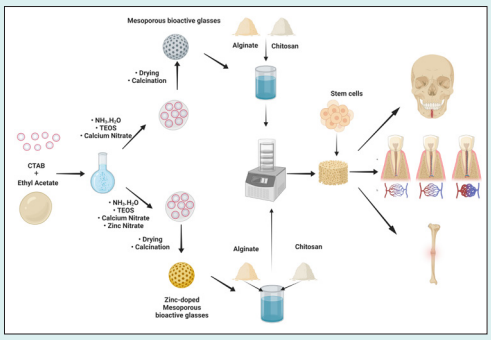

Methods: The Sol-Gel process was utilized for the synthesis of MBG and zinc-doped MBG (Zn-MBG), the latter being integrated into alginate/chitosan scaffolds which in turn were cross-linked to strengthen mechanical properties, followed by freeze-drying. The scaffold's physicochemical characterizations were evaluated, followed by investigations of its antioxidant properties, swelling behavior, mechanical properties, and porosity. The capacity of these biomaterials to increase cell viability and growth of apical papilla stem cells (SCAPs) and hemocompatibility was assessed as a final step.

Results: All fabricated scaffolds demonstrated proper porosity, biocompatibility, and hemocompatibility. Nanocomposite scaffolds with Zn-MBG presented a significant enhancement in cell viability for SCAPs compared to alginate/chitosan scaffolds. DPPH tests indicated that the Zn-MBG-alginate/chitosan scaffold showed the highest antioxidant properties.

Conclusion: Zn-MBG-alginate/chitosan nanocomposite scaffolds demonstrated great physicochemical characteristics and biological and mechanical properties, marking them as suitable candidates for dental root tissue engineering.

Introduction

Endodontic reconstruction focuses on repairing or promoting the regeneration of damaged or necrotic pulp tissue. Even though current root canal therapies have a high success rate, the ultimate aim is to reconstruct the tooth by replacing necrotic pulp with healthy tissue. This strategy aims to preserve both the tooth's function and structure, resulting in optimal oral health.[1] Tissue engineering utilizes a combination of scaffolds, cells, and growth factors to restore, improve or regenerate various tissues. Thus, it offers a promising approach in dentistry. Pulp tissue engineering, a subset of regenerative dentistry, targets the restoration of damaged or unhealthy dental pulp which is the soft tissue within the tooth containing blood vessels, nerves, and stem cells. This approach employs scaffolds, cells, and growth factors to regenerate functional pulp tissue, thereby supporting the tooth's vitality and sensitivity.

Stem cells are instrumental in tissue engineering because of their remarkable capacity for differentiation into diverse cell types. These cells are responsible for tissue renewal and reconstruction throughout the body, including the repair of damaged or necrotic tissues.[2] Apical papilla stem cells (SCAPs) can differentiate into odontoblasts and osteoblasts, the cells that produce dentin and bone, respectively. SCAPs also have a high proliferation rate, self-renewal capacity, and immunomodulatory properties.[3-5] SCAPS, which share a

*Corresponding author: Esmaeel Sharifi, Email: Esmaeel.sharifi@gmail.com

neural crest lineage with craniofacial tissues, represent a valuable source for craniofacial tissue regeneration due to their cellular homology.[6] These specialized stem cells play a vital role in tooth development and subsequent pulp regeneration within permanent teeth with open root ends. Notably, SCAPs can differentiate into dental pulp cells (DPSCs) and primary odontoblasts which makes them a promising candidate for dental pulp regeneration.[7] Their regenerative potential shows significant promise for advancements in dental therapies and enhanced tooth repair strategies.[6,7]

Furthermore, scaffolds offer a supportive substrate for cell adhesion and organization. By mimicking the native extracellular matrix, they serve to guide tissue development.[8] Scaffolds are critical elements in damaged tissue regeneration. They mimic the extracellular matrix. Additionally, scaffolds serve as delivery systems for growth factors and other maintenance factors that promote stem cell activity and they can be fabricated from diverse materials, including polymers and ceramics.[9] Natural polymeric scaffolds, particularly those derived from biocompatible and biodegradable materials with minimal immunogenicity are better suited for bone tissue engineering applications. Alginate, an edible heteropolysaccharide naturally extracted from brown seaweed (Phaeophyceae) is a prime example.[10] Alginate's biocompatibility, biodegradability, and hydrophilicity render it a versatile material for diverse tissue engineering applications.[11,12] Chitosan, a deacetylated derivative of chitin and the primary component of crustaceans, insects, and some fungal exoskeletons belongs to the class of natural polysaccharides.[13] Chitosan exhibits many properties. Biocompatibility, biodegradability, and inherent antimicrobial activity make it a compelling candidate for tissue-engineered scaffolds.[14,15]

MBG presents advantageous assets, including high surface area, controllable pore size, tunable composition, bioactivity, biodegradability, and the capacity for drug delivery.[16,17] MBGs exhibit the ability to induce hydroxyapatite formation on their surfaces upon exposure to physiological fluids. Furthermore, MBGs possess the ability to release calcium, phosphate, and silicate ions, thus promoting the odontogenic/osteogenic potential of DPSCs and stimulating dentin regeneration.[16]

Zinc is a crucial trace element and participates in diverse biological processes, including immune function, wound healing, and bone development. Notably, zinc exhibits both antibacterial and angiogenic properties. Composite scaffolds incorporating zinc and Mg-doped bioactive glass demonstrate remarkable antibacterial efficacy which is attributed to their ion release capacity.[18] Haider et al report the development of strontium- and zinc-doped bioglass (BG)-alginate composite scaffolds. These scaffolds exhibit a desirable combination of bioactivity, porosity, and mechanical stability. Notably, BG incorporation significantly improved the scaffold's compressive strength. Furthermore, the composites demonstrated sustained release of zinc, calcium, and strontium ions in Tris/HCl buffer, suggesting potential in vivo bioactivity and promotion of bone formation.[19] Huang et al investigated the influence of zinc and zinc-doped bioactive glasses on the odontogenic differentiation potential of human DPSCs. Synthesized zinc-doped BGs were assessed for their ability to induce mineralization and promote odontogenic differentiation. The findings revealed that free zinc ions (0-5 ppm) significantly enhanced both DPSCs proliferation and alkaline phosphatase activity. Notably, long-term treatment with zinc-doped BGs promoted the development of mineralized nodules in a similar vein as hydroxyapatite.[20] Tabari et al investigated the cytotoxic effects of four metal oxide nanoparticles (titanium, silicon, zinc, and aluminum) on human DPSCs. Their study revealed dose- and time-dependent cytotoxicity across the tested nanoparticles. Notably, all nanoparticles induced cell death and morphological alterations within the concentration range of 25-100 µg/ml.[21] Materials such as Zn-MBGs have emerged as promising tools for dental and craniofacial tissue engineering, often used in combination with apical papilla stem cells (APSCs). Notably, Zn-MBG nanoparticles exhibit the ability to increase the osteogenic/odontogenic differentiation of SCAPs. This effect may be due to the sustained release of zinc ions and bioactive molecules, which stimulate the expression of genes and proteins associated with osteogenesis and odontogenesis.[3]

Alginate-chitosan scaffolds incorporating Zn-MBG represent a promising multifunctional platform for regenerative medicine applications. This nanocomposite design synergistically leverages the properties of each biomaterial to promote the repair and regeneration of damaged tissues, including bone and dental pulp. However, optimizing scaffold composition, structure, and degradation kinetics remains crucial. Additionally, long-term biocompatibility evaluation is essential. Notably, Zn-MBG offers a versatile platform for pulp tissue engineering due to its combined bioactivity, mechanical support, and drug delivery capabilities. Addressing limitations in scaffold design, optimizing material compositions, and ensuring robust safety profiles are paramount for successful tissue regeneration. Furthermore, the successful clinical translation of these scaffolds necessitates overcoming technical, biological, and regulatory hurdles. Establishing clinically relevant manufacturing processes, demonstrably safe and sterile products and ensuring long-term stability are all critical for the commercialization of these tissue engineering technologies.[22] Looking ahead, scaffolds will continue to play a critical role in advancing tissue engineering.[23]

In the present study, the significance of a nanocomposite scaffold composed of chitosan and alginate which

incorporated zinc-doped MBG nanoparticles was studied on the growth and proliferation of SCAPs.

Materials and methods

Synthesis of MBG nanoparticles by the Sol-Gel method

The sol-gel method was utilized for the synthesis of MBG nanoparticles. This process involved synthesizing both MBG and Zn-MBG (where zinc replaces calcium ions within the MBG structure). The creation began with the addition of 2.24 g of CTAB (cetyltrimethylammonium bromide) to 104 mL of deionized water. This mixture underwent stirring for 30 min at 30 °C using a magnetic stirrer until a clear solution resulted. The subsequent step involved the gradual addition of 32 mL of ethyl acetate dropwise to the reaction solution, followed by another 30 min of magnetic stirring. The solution's pH was then adjusted to an alkaline state using ammonia and 23 mL of tetraethoxysilane (TEOS) was added dropwise. After 30 min, 5.21 g of calcium nitrate was incorporated into the reaction mixture for MBG synthesis. To achieve zinc substitution in the Zn-MBG structure, the synthesis utilized a combination of 4.34 g of zinc nitrate and a reduced amount of calcium nitrate (1.09 g). The reaction mixture then underwent stirring at room temperature for 4 h, followed by nanoparticle separation via centrifugation (9000 rpm for 10 min). Finally, the nanoparticles were aged at 60 °C for 16 h and calcined in a furnace at 700 °C. The protocol for synthesizing Zn-MBG is similar, with the only difference being the use of the aforementioned amounts of calcium nitrate and zinc nitrate to replace calcium ions with zinc ions within the MBG structure.[24]

Fabrication of scaffolds

To create the hydrogel scaffold, a uniform blend of alginate and chitosan polymers was first prepared.[25] This involved combining 25 mL of a 5% Wt./V alginate solution (prepared in double-distilled water) with 25 mL of a 5% Wt./V chitosan solution (prepared in 2% acetic acid). An identical procedure was used for fabricating the nanocomposite scaffolds. In the final stage, 20% Wt./V of either MBG or Zn-MBG nanoparticles were incorporated into the polymeric solution. The mixture underwent thorough mixing on a magnetic stirrer to achieve a completely homogenous state. To improve the mechanical strength of the resulting scaffolds, 1% V/V glutaraldehyde was added to each polymer mixture for in-situ crosslinking. The mixture was then stirred using a magnetic stirrer for 30 minutes and subsequently degassed using an ultrasonic bath. Following this, the prepared mixture was transferred to a mold and subjected to a gradual freezing process (1 h at 4°C, 16 h at -20°C, and 5 h at -70°C). Finally, the fabricated scaffolds were cut with a 5 mm biopsy punch, and slices with a thickness ranging from 2 to 10 mm were obtained from the freeze-dried samples for further analysis.

Characterization of synthesized nanoparticles

A high-resolution imaging technique known as Field Emission Scanning Electron Microscopy (FESEM, MIRA3) was utilized to examine the surface characteristics and particle size of the MBG and Zn-MBG nanoparticles. ImageJ software served as the tool for estimating the particle size. Energy-dispersive X-ray spectroscopy (EDS) was employed to analyze the elemental composition of the synthesized nanoparticles and to verify the presence of the desired ions within the MBG structure. Fourier transform infrared spectroscopy (FTIR) (Bruker) was used to identify the functional groups present in the synthesized MBGs. This involved mixing the sample with potassium bromide (KBr) powder in a 1:40 ratio. The resulting mixture was then compressed and analyzed at a frequency of 2.60 Hz within the wavenumber range of 400-4000 cm^{-1}. X-ray diffraction (XRD) was employed to determine the crystalline or amorphous structure and phases present in the synthesized MBGs. This technique involved recording the diffraction pattern of the MBGs across a range of angles (2θ) from 10 to 70 degrees.[25]

Characterization of fabricated nanocomposite scaffolds

The examination of the scaffolds' surface characteristics and internal pore structure, along with the elemental distribution throughout the fabricated scaffolds, was conducted using a scanning electron microscope (SEM) coupled with EDS (X MIRA3, Tescan, Brno, Czech Republic). FTIR, performed using a Bruker-IFS48 instrument, was employed to identify the functional groups present within the scaffolds. An assessment of the mechanical properties and compressive strength of the prepared scaffolds (measuring 10x20 mm) was carried out using a compressive strength test. The SANTAM model STM-2, manufactured in Iran, was utilized for this purpose.[9]

Evaluation of scaffolds antioxidant properties

The free radical scavenging capacity of the prepared scaffolds was evaluated with the DPPH radical scavenging assay. A solution containing the fabricated nanocomposite scaffolds (20 mg of scaffolds appropriately immersed in 1 mL of methanol) was prepared in a 1:1 ratio with DPPH solution (80 µg/mL), serving as the source of free radicals. The samples were incubated in darkness at room temperature (maintained at 25 °C with a tolerance of plus or minus 1 °C) for 30 min. Following incubation, the neutralization of DPPH compared to the negative control was measured at a wavelength of 517 nanometers using a Shimadzu UV-1800 spectrophotometer, as described by the following equation:

$$SC\% = \frac{OD_n - OD_S}{OD_n} \times 100$$

In this context, OD_n represents the absorbance of the

control reaction, while OD_S corresponds to the absorbance of the sample.[26]

Biocompatibility and hemocompatibility

The prepared scaffolds' cytotoxicity is evaluated using the MTT assay against SCAPs cells. To achieve this, the freeze-dried scaffolds were sterilized with 70% v/v ethanol followed by UV light exposure. Subsequently, they were incubated in α-MEM medium for 24 hours at 37°C. The next step involved seeding 1 x 10^4 SCAPs cells (passage 4) onto the top of each scaffold. The cell culture medium used contained 1% penicillin streptomycin and 15% FBS. The plates were then placed in an incubator set at 37°C with 5% CO2 and 95% humidity for 1 and 3 days. Following each desired incubation period, 10 µL of MTT solution was added to each well. The plate was then incubated for 3.5 hours at 37°C. This was followed by the addition of 100 µL DMSO to dissolve the formazan crystals formed. After 5 minutes of adding DMSO, the medium was transferred to a 96-well plate and the optical density (OD) was measured at a wavelength of 595 nm using a microplate reader) Stat Fax 4300). The hemocompatibility of the prepared scaffolds was evaluated similarly to our previous study.[27]

Statistical analysis

SPSS version 18 was used for data analysis. Differences in the parameters of all groups have been evaluated by ANOVA analysis.

Results

Characterization of nanoparticles

The diffraction pattern of MBGs in the ranges of 10 to 70 and angles of 2θ was shown in Fig. 1. XRD spectrum revealed similar patterns for both nanoparticles. Notably, a broad band across 20-34° 2θ can be attributed to amorphous silicate, signifying the amorphous nature of both samples.[24]

FTIR spectra of both MBG nanoparticles are shown in Fig. 2. The characteristic bands, notably located at 1000 to 1250/cm comprise a sharp peak attributed to the Si-O-Si stretching vibrational mode at 1090/cm. Furthermore, a characteristic vibrational band of Si-O-Si was detected around 800/cm. Another Si-O-Si band was identified at approximately 470/cm. No significant variations in the molecular structure of Zn-MBG were observed following the doping of zinc in the MBG structure at the FTIR spectrum.[24]

The FESEM image is shown in Fig. 3. The size of MBG and Zn-MBG were 80 nm and 30 nm, respectively. Doping of zinc into the MBG structure reduced the nanoparticle size. Additionally, the effectiveness of zinc doping was verified via EDS analysis (Fig. 3), a technique that determines elemental distribution within the samples.

DLS/zeta was used to determine the size distribution,

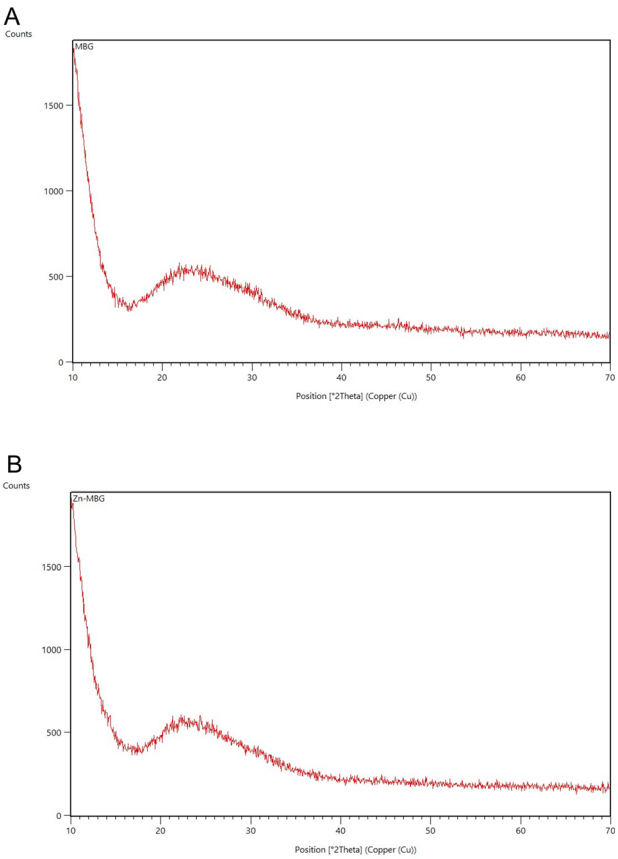

Fig. 1. XRD pattern of MBG (A) and Zn-MBG (B).

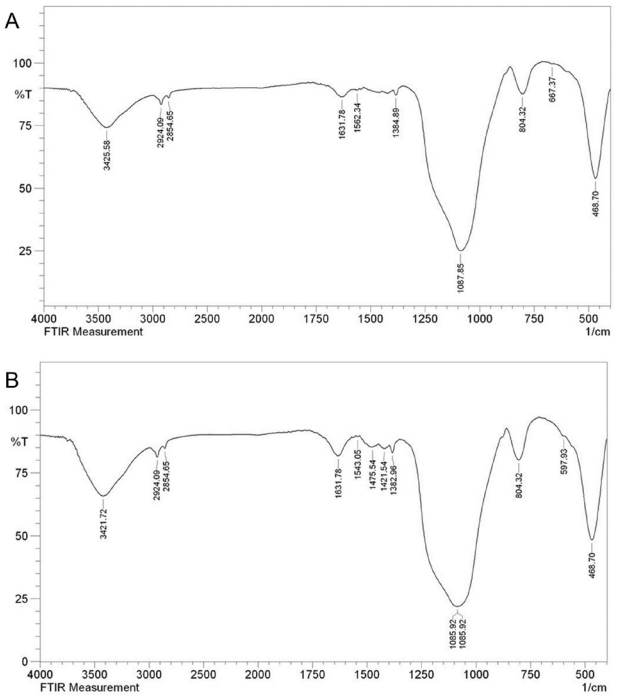

Fig. 2. FTIR spectrum of MBG (A) and Zn-MBG (B).

hydrodynamic diameter, and surface charge of the MBG. Notably, a broad peak was observed for both types, which could be attributed to aggregations of MBGs and their partial dispersion. This is consistent with the findings

observed in the FESEM images. The average hydrodynamic diameter and zeta potential of MBG were 448.5 nm, and -15.3 mV, while for Zn-MBG, the average diameter was 85.86 nm, and -10.7 mV, respectively (Fig. 4).

Scaffolds characterizations

The infrared (FTIR) spectra of Alg/Cs, Alg/Cs-MBG, and Alg/Cs-MBG/Zn scaffolds are shown in Fig. 5. In the Alg/Cs scaffold, the peaks located between 3400 and 3600 cm^{-1} indicate the presence of O-H (hydroxyl) bonds. The peak at 1600 cm^{-1} corresponds to the N-H (amine) bending vibration and the peak at 1450 cm^{-1} represents the COO- (carboxylate) or C = O (carbonyl) groups.

The morphology, porosity, and elemental distribution of the scaffolds were assessed by a SEM coupled with an EDS analyzer. As represented in Fig. 6, SEM images showed scaffolds porous structure. The porous and rough surface of these scaffolds provided an ideal environment for cell adhesion and cell proliferation. As per data obtained from ImageJ, the average pore size was between 120, 180 and 217 µm for Alg /Cs, Alg /Cs-MBG, and Alg /Cs-MBG/Zn scaffolds respectively. The elemental analysis of the constructed scaffolds revealed the following constituent elements within the fabricated scaffolds; Alg /Cs containing oxygen (O), carbon (C), nitrogen (N), Alg /Cs-MBG representing C, O, N and silicon (Si), as well as calcium (Ca) and the Alg /Cs-MBG/Zn scaffold containing C, O, N, Si, Ca and zinc (Zn).

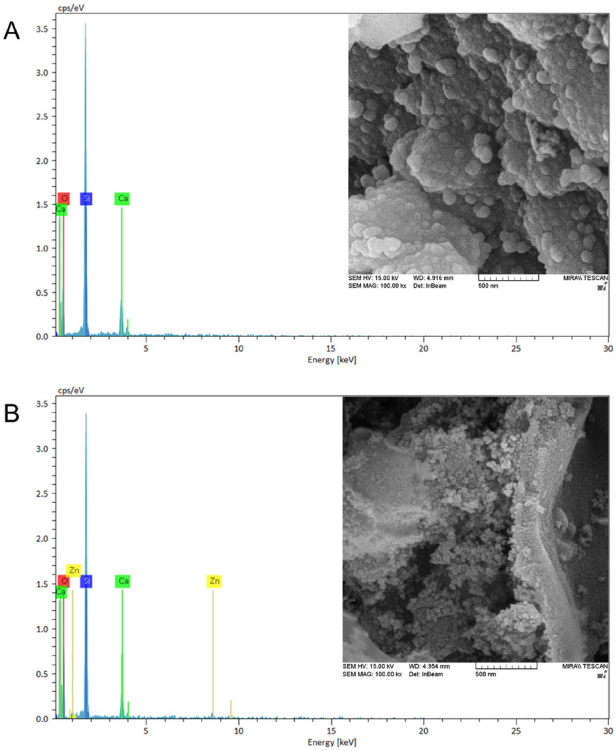

Fig. 3. Scanning electron microscope micrograph and relative EDS analysis of MBG (A) and MBG-Zn (B). (scale 500 nm).

Biocompatibility

In this study, the MTT method was used to assess the viability of cells on various scaffolds (Fig. 7A). The viability of SCAPs cells on the first and third day was assessed for the following scaffold types: Alg/Cs, Alg/Cs-MBG, and Alg/Cs-MBG/Zn, which were compared to the scaffold-less control group. MTT assay results demonstrated that Alg/Cs, Alg/Cs-MBG and Alg/Cs-MBG/Zn scaffolds exhibited favorable biocompatibility properties on the first and third day. Cell viability significantly increased as the scaffolds provided a 3D microenvironment for proliferation. Additionally, the addition of MBG and

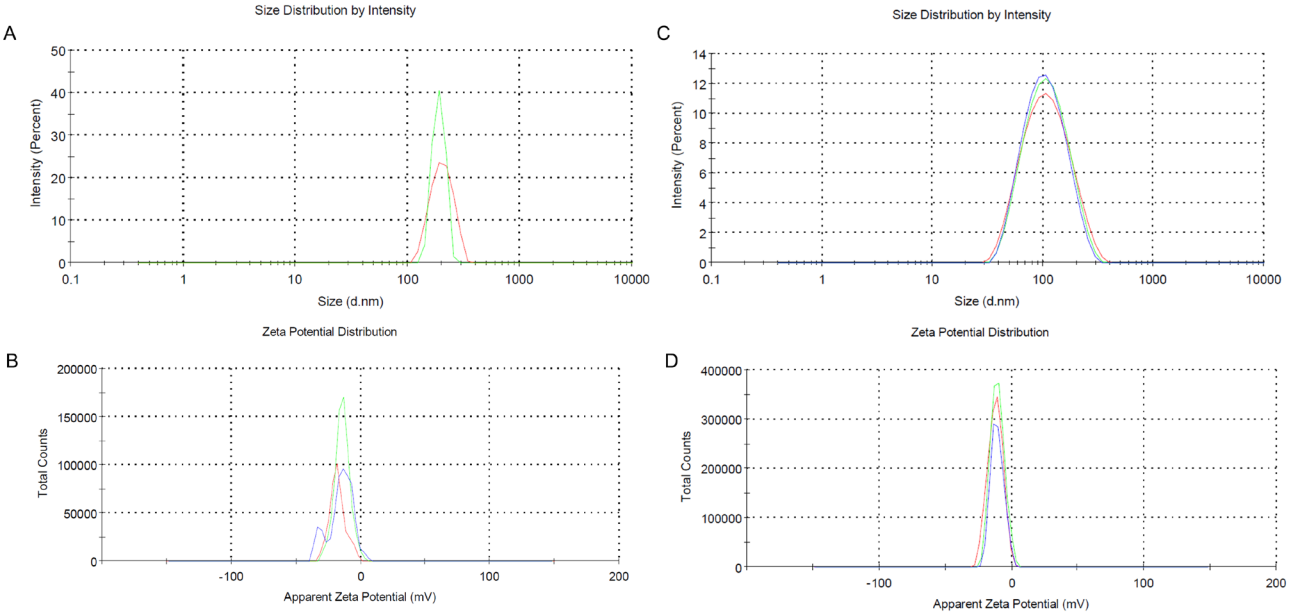

Fig. 4. DLS/Zeta of synthesized MBG NPs, the hydrodynamic diameter of MBG(A), the zeta potential of MBG NPs (B), the hydrodynamic diameter of Zn-MBG (C), and related zeta potential of Zn-MBG NPs (D).

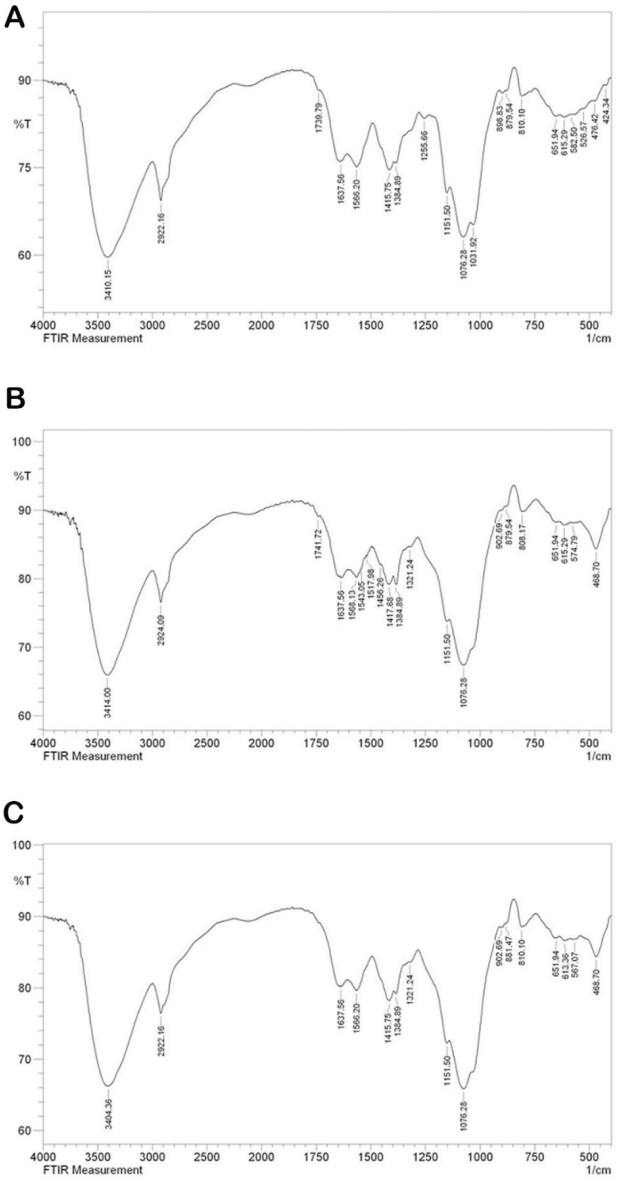

Fig. 5. FTIR spectrum of Alg/Cs (A), Alg/Cs-MBG (B), and Alg /Cs-MBG/Zn scaffolds (C).

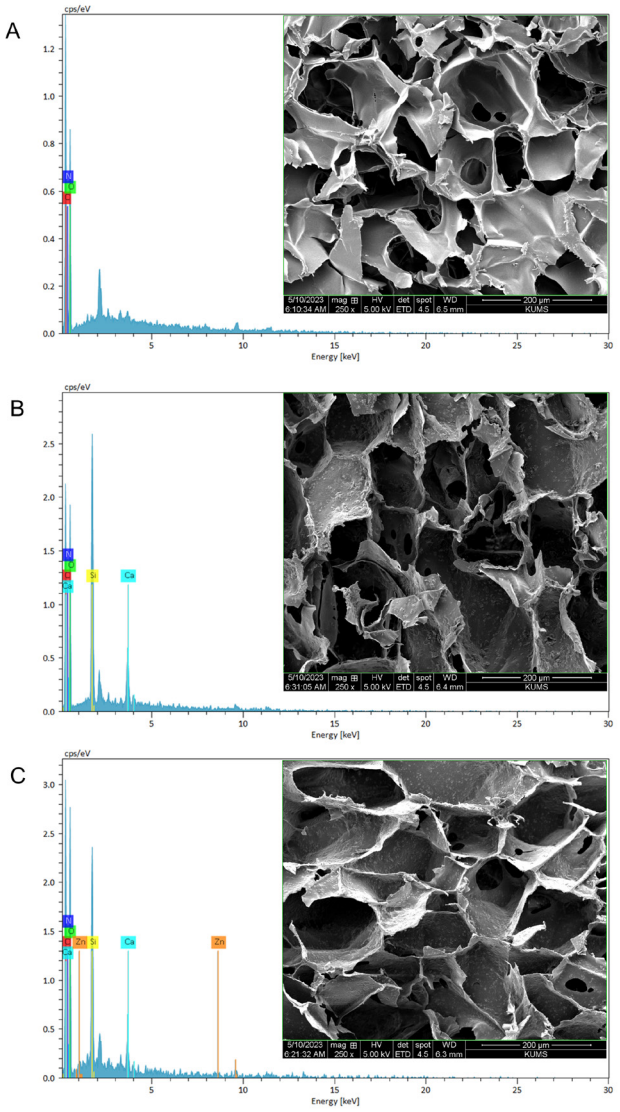

Fig. 6. SEM micrographs and EDS analysis of Alg/Cs scaffolds (A), Alg/Cs-MBG (B), and Alg /Cs-MBG/Zn (C) scaffolds (Scale 200 µm).

MBG/Zn enhanced cell viability compared to the neat scaffold. Notably, MBG/Zn exhibited elevated viability compared to the other scaffolds.

The hemolysis test results (Fig. 7B) demonstrate that the fabricated scaffolds were hemocompatible. Furthermore, the incorporation of MBG or Zn-MBG did not notably influence the lysis of red blood cells, compared to the Triton X100 as the control group.

Antioxidant properties

Fig. 8 presents the outcomes of the antioxidant property test utilizing DPPH, which confirms the antioxidant characteristics of the fabricated scaffolds. The addition of MBG and Zn-MBG enhanced the antioxidant properties of the scaffolds by 44.58% and 69.43%, respectively, as compared to the neat Alg/Cs scaffold.

Mechanical properties

The elastic modulus of the Alg/Cs scaffold was higher than other scaffolds, the addition of MBG and MBG-Zn nanoparticles in the scaffold decreased the scaffold's elastic modulus as anticipated. Table 1 presents the elastic modulus for the fabricated scaffolds.

Discussion

Treatment of immature root canals presents certain challenges such as reduced tooth sensitivity and vitality, susceptibility to secondary infections, and an increased risk of subsequent fractures. However, advancements in regenerative therapy offer a promising approach to restoring pulp-dentin tissue. To that end, a combination of mesenchymal stem cells, growth factors, and scaffolds is employed. Specifically, stem cells of apical papilla (SCAPs), which reside in the apical papilla of immature permanent teeth, play a crucial role. These SCAPs exhibit unique

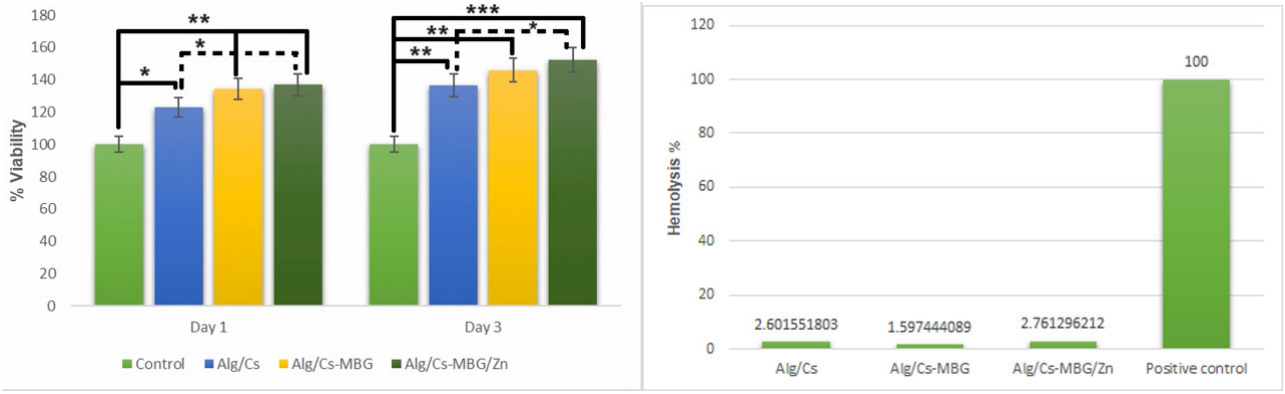

Fig. 7. Comparison of the cell survival of SCAPs and hemolysis rate in Alg/Cs, Alg/Cs-MBG, and Alg/Cs-MBG/ Zn scaffolds with the control group on days 1 and 3 (*P<05, ** P<01, ***P<001).

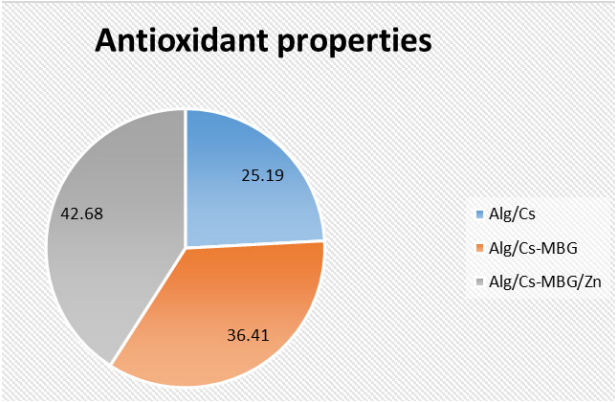

Fig. 8. Comparison of antioxidant properties in Alg/Cs, Alg/Cs-MBG, and Alg/Cs-MBG/Zn scaffolds.

characteristics, including high proliferation potential, self-renewal ability and low immunogenicity.[4,6,28]

In the present study, nanocomposite scaffolds were synthesized and their biological properties were assessed *in vitro* for dental tissue regeneration treatments. To that end, an Alg/Cs-MBG/Zn scaffold was chosen to enhance the regeneration of dental tissues.[29] In contrast to microparticles, nanoparticles offer an elevated level of bioactivity. Furthermore, the mesoporous structure of these particles enhances the surface area, resulting in more binding sites for cell adhesion and tissue formation.[30-32]

Based on the XRD pattern of the synthesized MBGs, it was found that the inspected material possessed an amorphous structure, consistent with previous findings.[24] Additionally, FTIR results further validated the synthesis of the aforementioned nanoparticles, with distinct bands associated with MBG being observed in the obtained spectra.[33,34] The combination of these analytical techniques provided valuable insights into the material's composition and structure, supporting the successful synthesis of MBGs.

DLS/Zeta analysis results indicate the Zn-MBG hydrodynamic diameter is less than neat MBG NPs diameter, and the zeta potential of Zn-MBG increased due to the zinc positive charge. In line with the DLS

Table 1. The mechanical properties of the prepared scaffolds

Scaffold	Alg/Cs-MBG/Zn	Alg/Cs-MBG	Alg/Cs
Elastic modulus	29.13	34.52	35.72

results, the FESEM images showed a decreased size of Zn-MBG NPs. EDS analysis yielded several valuable insights. 1-Zinc Doping, proper zinc doping was observed in the Zn-MBG structure. 2-Calcium Reduction, in comparison to synthesized MBG, the Zn-MBG exhibits a reduced calcium content. This reduction occurs because zinc replaces calcium during the synthesis process. 3-Impurity-free synthesis, the presence of Si, O, and Ca in the structure of the MBG confirms their purity. These synthesized MBGs are devoid of impurities.[18,35]

When comparing the FTIR spectrum of the fabricated scaffolds with other types, characteristic bonds of chitosan, alginate and MBG were observed. Additionally, EDS revealed the distribution of MBG or MBG/Zn elements throughout the scaffold structure contributed to its supportive surface properties for cell adhesion.[9]

Cell adhesion on polymer surfaces is influenced by several factors, including cell type, surface charge, and substrate surface roughness. Notably, both microscopic and submicron roughness, similar to what was observed in scaffolds fabricated in the present study, exhibited positive effects on cell adhesion and cell growth.[36] These observations were in alignment with results obtained from cytotoxicity and survival assessments. SEM images of the fabricated nanocomposite scaffolds revealed both the surface roughness and the porous structure of the scaffold. These features made the scaffold ideal for stem cell adhesion and growth.[36] Notably, uniform and homogeneous dispersion of MBG particles within the Alg/Cs-MBG/Zn composite scaffold structure is a critical attribute that any synthesized scaffold must possess to fulfill its intended role in tissue regeneration and repair effectively.[37,38] This well-designed scaffold holds promise for advancing tooth tissue regeneration and contributing to the field of biomedical engineering.

The interconnected pores in the scaffolds exhibited

a range of sizes, spanning from less than 50 μm to 500 μm. The average pore size was within the range of 120 to 217 μm. The porous structure of these scaffolds played a crucial role in cell migration, angiogenesis, nutrient/waste diffusion, and the formation of new tissues. For tissue engineering, the minimum suitable pore size is 75 μm, while the maximum acceptable pore size is 900 μm.[18]

According to the DPPH method, the addition of Zn-MBG, and MBG to the nanocomposite scaffolds, increased the antioxidant properties of fabricated scaffolds, and elevated antioxidant properties were seen in Zn-MBG scaffolds, due to the antioxidant properties of zinc. The mechanical strength of the nanocomposite showed improvements due to the incorporation of MBGs. While having a porosity ranging from 55% to 74%, the scaffolds maintained mechanical integrity. The degree of porosity, water absorption capacity and scaffold degradation significantly impacted their mechanical strength and biological activity. Ideally, scaffold degradation should occur concurrently with new tissue formation.[27,39] The ions released from the scaffold can trigger various cellular responses. Moreover, scaffolds play a role in stimulating stem cell proliferation and differentiation within their porous structure.[40]

The findings from the present study revealed that in Alg/Cs-MBG/Zn and Alg/Cs-MBG scaffolds, proliferation of SCAPs exhibited a significant increase on the first and third days, as compared to both the control group and the Alg/Cs scaffold. Notably, the highest survival rate was observed in cells seeded on the Alg/Cs-MBG/Zn scaffold, suggesting distinct cellular responses to varying materials. In a study by Moshiri et al, it was observed that gelatin and chitosan, when used individually, did not significantly contribute to bone ossification. However, the combination of biological materials in the form of a composite scaffold were necessary.[41] Various studies have demonstrated the beneficial impact of doping different elements into the structure of nanoparticles incorporated in the scaffolds. Zheng et al incorporated copper-doped bioactive glass nanoparticles into a gelatin scaffold containing 45S5. Their findings revealed an accelerated formation of an apatite layer on the scaffold's surface in the presence of BG nanoparticles containing copper after immersion in SBF.[42] In a study by Shoaib et al, it was seen that various concentrations of Mg-doped MBG nanoparticles did not show significant cytotoxic effects on NHFB despite reserved effect on the MG-63 cancer cell viability.[43] Similarly, the addition of strontium-doped MSN, into the chitosan/gelatin scaffolds exhibited favorable porosity and surface roughness, along with high biocompatibility.[25] Antibacterial alginate chitosan nanocomposite film with functionalized multiwalled carbon nanotubes and zinc oxide has potential use for biomedical applications.[44] Alginate chitosan scaffolds containing zinc-doped MBG apical papilla stem cells have been explored for various applications in tissue engineering, especially for dental and craniofacial regeneration. For example, these scaffolds can be used to support the growth and function of SCAPs and to induce the formation of vascularized and mineralized tissues in animal models.[45] These scaffolds can also release zinc ions and bioactive molecules that stimulate the expression of osteo/odontogenic genes and proteins in SCAPs.[46]

Of note, the present study showed that a 20% Wt./Wt. ratio of MBG and polymer not only was non-toxic but also enhanced the proliferation potential of the nanocomposite scaffold, compared to the control group. The current research findings highlight the positive effect of zinc doping in the structure of MBG, particularly in enhancing the survival and proliferation of SCAPs seeded on the nanocomposite scaffolds. When considering the industrial scalability of these nanocomposite scaffolds for dental root tissue regeneration, some substantial features must be considered, e.g., manufacturing process optimization, biocompatibility and safety (immune response, and investigating potential long-term safety of fabricated scaffold degradation products *in vivo)*, and confirming they meet regulatory standards.

Conclusion

In the present study, amorphous MBG and Zn-MBG nanoparticles were synthesized by the sol-gel process. To create the nanocomposite scaffold, chitosan and alginate were utilized, which caused the incorporation of the MBG and Zn-MBG nanoparticles into the hydrogel. The scaffolds exhibited appropriate porosity, antioxidant properties, and mechanical characteristics. These scaffolds were both biocompatible and hemocompatible. Notably, the Alg/Cs-MBG/Zn scaffolds provided a suitable microenvironment for cell proliferation and viability. The findings of the present study indicate that the Alg/Cs-MBG/Zn nanocomposite scaffold could serve as an ideal microenvironment for the proliferation and differentiation of SCAPs. While Alg/Cs-MBG/Zn nanocomposite scaffolds hold promise, addressing the study limitations such as assessment of their overall biocompatibility with surrounding tissues and immune responses should be thoroughly evaluated, and explore surface functionalization techniques to enhance specific interactions with stem cells, such as incorporating growth factors or peptides onto the scaffold surface will contribute to their successful clinical translation in dental regenerative medicine.

Acknowledgments

The authors greatly acknowledge the vice chancellor of Hamadan University of Medical Sciences for supporting the finalization of this study.

Authors' Contribution

Conceptualization: Elham Khoshbin, Morteza Jalilvand, Esmaeel

Research Highlights

What is the current knowledge?

- MBG nanoparticles are biocompatible and biodegradable biomaterials.
- Nanocomposite scaffolds based on alginate and chitosan comprising MBG have potential applications for bone tissue engineering.

What is new here?

- Zinc-doped MBGs were synthesized successfully.
- Nanocomposite scaffolds containing zinc-doped MBGs were synthesized successfully and showed biomaterial characteristics as well as proper biocompatibility and hemocompatibility.

Sharifi, Hamed Karkehabadi.
Data curation: Elham Khoshbin, Morteza Jalilvand, Zahra Barabadi, Esmaeel Sharifi.
Formal analysis: Morteza Jalilvand, Zahra Barabadi, Esmaeel Sharifi, Hamed Karkehabadi
Funding acquisition: Elham Khoshbin.
Investigation: Morteza Jalilvand, Zahra Barabadi, Esmaeel Sharifi, Hamed Karkehabadi.
Methodology: Elham Khoshbin, Morteza Jalilvand, Zahra Barabadi, Esmaeel Sharifi, Hamed Karkehabadi.
Project administration: Elham Khoshbin, Esmaeel Sharifi, Hamed Karkehabadi.
Resources: Elham Khoshbin, Morteza Jalilvand, Zahra Barabadi, Esmaeel Sharifi, Hamed Karkehabadi.
Supervision: Elham Khoshbin, Zahra Barabadi, Esmaeel Sharifi, Hamed Karkehabadi.
Validation: Elham Khoshbin, Zahra Barabadi, Esmaeel Sharifi, Hamed Karkehabadi.
Visualization: Morteza Jalilvand, Zahra Barabadi, Esmaeel Sharifi, Hamed Karkehabadi.
Writing–original draft: Elham Khoshbin, Morteza Jalilvand, Zahra Barabadi, Esmaeel Sharifi.
Writing–review & editing: Elham Khoshbin, Esmaeel Sharifi, Hamed Karkehabadi.

Competing Interests

The authors declare no conflicts of interest.

Ethical Statement

The study was approved by the ethics committee of Hamadan University of Medical Sciences (IR.UMSHA.REC.1401.741).

Funding

Elham Khoshbin acquired the grant from Hamadan University of Medical Sciences (Grant number: 140109228222).

References

1. Belli S, Eraslan O, Eskitascioglu G. Direct restoration of endodontically treated teeth: a brief summary of materials and techniques. *Curr Oral Health Rep* **2015**; 2: 182-9. doi: 10.1007/s40496-015-0068-5.
2. Sharifi E, Chehelgerdi M, Fatahian-Kelishadrokhi A, Yazdani-Nafchi F, Ashrafi-Dehkordi K. Comparison of therapeutic effects of encapsulated mesenchymal stem cells in *Aloe vera* gel and chitosan-based gel in healing of grade-II burn injuries. *Regen Ther* **2021**; 18: 30-7. doi: 10.1016/j.reth.2021.02.007.
3. Rakhimova O, Schmidt A, Landström M, Johansson A, Kelk P, Romani Vestman N. Cytokine secretion, viability, and real-time proliferation of apical-papilla stem cells upon exposure to oral bacteria. *Front Cell Infect Microbiol* **2020**; 10: 620801. doi: 10.3389/fcimb.2020.620801.
4. Liu Q, Gao Y, He J. Stem cells from the apical papilla (SCAPs): past, present, prospects, and challenges. *Biomedicines* **2023**; 11: 2047. doi: 10.3390/biomedicines11072047.
5. Nagata M, Ono N, Ono W. Unveiling diversity of stem cells in dental pulp and apical papilla using mouse genetic models: a literature review. *Cell Tissue Res* **2021**; 383: 603-16. doi: 10.1007/s00441-020-03271-0.
6. Liu Y, Zhuang X, Yu S, Yang N, Zeng J, Liu X, et al. Exosomes derived from stem cells from apical papilla promote craniofacial soft tissue regeneration by enhancing Cdc42-mediated vascularization. *Stem Cell Res Ther* **2021**; 12: 76. doi: 10.1186/s13287-021-02151-w.
7. Kang J, Fan W, Deng Q, He H, Huang F. Stem cells from the apical papilla: a promising source for stem cell-based therapy. *Biomed Res Int* **2019**; 2019: 6104738. doi: 10.1155/2019/6104738.
8. Eltom A, Zhong G, Muhammad A. Scaffold techniques and designs in tissue engineering functions and purposes: a review. *Adv Mater Sci Eng* **2019**; 2019: 3429527. doi: 10.1155/2019/3429527.
9. Yousefiasl S, Manoochehri H, Makvandi P, Afshar S, Salahinejad E, Khosraviyan P, et al. Chitosan/alginate bionanocomposites adorned with mesoporous silica nanoparticles for bone tissue engineering. *J Nanostruct Chem* **2023**; 13: 389-403. doi: 10.1007/s40097-022-00507-z.
10. Sahoo DR, Biswal T. Alginate and its application to tissue engineering. *SN Appl Sci* **2021**; 3: 30. doi: 10.1007/s42452-020-04096-w.
11. Sreya ES, Kumar DP, Balakrishnan P, Gopi S. Science and technology of alginates: a review. In: *Handbook of Biomass*. Springer; **2023**. p. 1-28. doi: 10.1007/978-981-19-6772-6_48-1.
12. Kumar A, Kothari A, Kumar P, Singh A, Tripathi K, Gairolla J, et al. Introduction to alginate: biocompatible, biodegradable, antimicrobial nature and various applications. In: *Alginate-Applications and Future Perspectives*. Rijeka: IntechOpen; **2023**. doi: 10.5772/intechopen.110650.
13. Piekarska K, Sikora M, Owczarek M, Jóźwik-Pruska J, Wiśniewska-Wrona M. Chitin and chitosan as polymers of the future-obtaining, modification, life cycle assessment and main directions of application. *Polymers (Basel)* **2023**; 15: 793. doi: 10.3390/polym15040793.
14. Amirthalingam S, Rajendran AK, Mani P, Rangasamy J. Perspectives and challenges of using chitosan in various biological applications. In: Jayakumar R, Prabaharan M, eds. *Chitosan for Biomaterials III*. Vol 287. Cham: Springer International Publishing; **2021**. p. 1-22. doi: 10.1007/12_2021_107.
15. Desai R, Pachpore R, Patil A, Jain R, Dandekar P. Review of the structure of chitosan in the context of other sugar-based polymers. In: Jayakumar R, Prabaharan M, eds. *Chitosan for Biomaterials III*. Vol 287. Cham: Springer International Publishing; **2021**. p. 23-74. doi: 10.1007/12_2021_89.
16. Baino F. Copper-doped ordered mesoporous bioactive glass: a promising multifunctional platform for bone tissue engineering. *Bioengineering (Basel)* **2020**; 7: 45. doi: 10.3390/bioengineering7020045.
17. Huang W, Yang J, Feng Q, Shu Y, Liu C, Zeng S, et al. Mesoporous bioactive glass nanoparticles promote odontogenesis and neutralize pathophysiological acidic pH. *Front Mater* **2020**; 7: 241. doi: 10.3389/fmats.2020.00241.
18. Zamani D, Moztarzadeh F, Bizari D. Alginate-bioactive glass containing Zn and Mg composite scaffolds for bone tissue engineering. *Int J Biol Macromol* **2019**; 137: 1256-67. doi: 10.1016/j.ijbiomac.2019.06.182.
19. Haider A, Waseem A, Karpukhina N, Mohsin S. Strontium- and zinc-containing bioactive glass and alginates scaffolds. *Bioengineering (Basel)* **2020**; 7: 10. doi: 10.3390/bioengineering7010010.
20. Huang M, Hill RG, Rawlinson SC. Zinc bioglasses regulate mineralization in human dental pulp stem cells. *Dent Mater* **2017**; 33: 543-52. doi: 10.1016/j.dental.2017.03.011.
21. Tabari K, Hosseinpour S, Parashos P, Kardouni Khozestani P, Mohammad-Rahimi H. Cytotoxicity of selected nanoparticles on

human dental pulp stem cells. *Iran Endod J* **2017**; 12: 137-42. doi: 10.22037/iej.2017.28.
22. Meena P, Kakkar A, Kumar M, Khatri N, Nagar RK, Singh A, et al. Advances and clinical challenges for translating nerve conduit technology from bench to bed side for peripheral nerve repair. *Cell Tissue Res* **2021**; 383: 617-44. doi: 10.1007/s00441-020-03301-x.
23. Webber MJ, Khan OF, Sydlik SA, Tang BC, Langer R. A perspective on the clinical translation of scaffolds for tissue engineering. *Ann Biomed Eng* **2015**; 43: 641-56. doi: 10.1007/s10439-014-1104-7.
24. Neščáková Z, Zheng K, Liverani L, Nawaz Q, Galusková D, Kaňková H, et al. Multifunctional zinc ion doped sol - gel derived mesoporous bioactive glass nanoparticles for biomedical applications. *Bioact Mater* **2019**; 4: 312-21. doi: 10.1016/j.bioactmat.2019.10.002.
25. Yousefiasl S, Manoochehri H, Sharifi E. Strontium-doped mesoporous silica nanoparticles incorporated in chitosan/alginate biocomposite scaffolds for enhanced bone tissue regeneration. *Polym Adv Technol* **2023**; 34: 2322-34. doi: 10.1002/pat.6053.
26. Bagheri M, Validi M, Gholipour A, Makvandi P, Sharifi E. Chitosan nanofiber biocomposites for potential wound healing applications: antioxidant activity with synergic antibacterial effect. *Bioeng Transl Med* **2022**; 7: e10254. doi: 10.1002/btm2.10254.
27. Sharifi E, Sadati SA, Yousefiasl S, Sartorius R, Zafari M, Rezakhani L, et al. Cell loaded hydrogel containing Ag-doped bioactive glass-ceramic nanoparticles as skin substitute: antibacterial properties, immune response, and scarless cutaneous wound regeneration. *Bioeng Transl Med* **2022**; 7: e10386. doi: 10.1002/btm2.10386.
28. Tatullo M, Marrelli M, Shakesheff KM, White LJ. Dental pulp stem cells: function, isolation and applications in regenerative medicine. *J Tissue Eng Regen Med* **2015**; 9: 1205-16. doi: 10.1002/term.1899.
29. Sonoyama W, Liu Y, Fang D, Yamaza T, Seo BM, Zhang C, et al. Mesenchymal stem cell-mediated functional tooth regeneration in swine. *PLoS One* **2006**; 1: e79. doi: 10.1371/journal.pone.0000079.
30. Andishmand H, Azadmard-Damirchi S, Hamishekar H, Torbati M, Kharazmi MS, Savage GP, et al. Nano-delivery systems for encapsulation of phenolic compounds from pomegranate peel. *Adv Colloid Interface Sci* **2023**; 311: 102833. doi: 10.1016/j.cis.2022.102833.
31. Andishmand H, Yousefi M, Jafari N, Azadmard-Damirchi S, Homayouni-Rad A, Torbati M, et al. Designing and fabrication of colloidal nano-phytosomes with gamma-oryzanol and phosphatidylcholine for encapsulation and delivery of polyphenol-rich extract from pomegranate peel. *Int J Biol Macromol* **2024**; 256: 128501. doi: 10.1016/j.ijbiomac.2023.128501.
32. Yousefi M, Andishmand H, Assadpour E, Barzegar A, Kharazmi MS, Jafari SM. Nanoliposomal delivery systems of natural antibacterial compounds; properties, applications, and recent advances. *Crit Rev Food Sci Nutr* **2023**; 1-14. doi: 10.1080/10408398.2023.2170318.
33. Eid MM. Characterization of nanoparticles by FTIR and FTIR-microscopy. In: *Handbook of Consumer Nanoproducts*. Singapore: Springer; **2021**. p. 1-30. doi: 10.1007/978-981-15-6453-6_89-1.
34. Siqueira RL, Costa LC, Schiavon MA, de Castro DT, dos Reis AC, Peitl O, et al. Bioglass® and resulting crystalline materials synthesized via an acetic acid-assisted sol–gel route. *J Solgel Sci Technol* **2017**; 83: 165-73. doi: 10.1007/s10971-017-4402-3.
35. Vukajlovic D, Novakovic K, Bretcanu O. Self-crystallisation, an unexpected property of 45S5 Bioglass®. *Chem Commun (Camb)* **2021**; 57: 13558-61. doi: 10.1039/d1cc04847c.
36. Cai S, Wu C, Yang W, Liang W, Yu H, Liu L. Recent advance in surface modification for regulating cell adhesion and behaviors. *Nanotechnol Rev* **2020**; 9: 971-89. doi: 10.1515/ntrev-2020-0076.
37. Gómez-Cerezo MN, Peña J, Ivanovski S, Arcos D, Vallet-Regí M, Vaquette C. Multiscale porosity in mesoporous Bioglass 3D-printed scaffolds for bone regeneration. *Mater Sci Eng C Mater Biol Appl* **2021**; 120: 111706. doi: 10.1016/j.msec.2020.111706.
38. Grigora ME, Terzopoulou Z, Baciu D, Steriotis T, Charalambopoulou G, Gounari E, et al. 3D printed poly(lactic acid)-based nanocomposite scaffolds with bioactive coatings for tissue engineering applications. *J Mater Sci* **2023**; 58: 2740-63. doi: 10.1007/s10853-023-08149-4.
39. Sharifi E, Yousefiasl S, Laderian N, Rabiee N, Makvandi P, Pourmotabed S, et al. Cell-loaded genipin cross-linked collagen/gelatin skin substitute adorned with zinc-doped bioactive glass-ceramic for cutaneous wound regeneration. *Int J Biol Macromol* **2023**; 251: 125898. doi: 10.1016/j.ijbiomac.2023.125898.
40. Nikolova MP, Chavali MS. Recent advances in biomaterials for 3D scaffolds: A review. *Bioact Mater.* **2019**;4:271-292. doi: 10.1016/j.bioactmat.2019.10.005.
41. Moshiri A, Tekyieh Maroof N, Mohammad Sharifi A. Role of organic and ceramic biomaterials on bone healing and regeneration: an experimental study with significant value in translational tissue engineering and regenerative medicine. *Iran J Basic Med* Sci **2020**; 23: 1426-38. doi: 10.22038/ijbms.2020.46228.10707.
42. Zheng K, Wu J, Li W, Dippold D, Wan Y, Boccaccini AR. Incorporation of Cu-containing bioactive glass nanoparticles in gelatin-coated scaffolds enhances bioactivity and osteogenic activity. *ACS Biomater Sci Eng* **2018**; 4: 1546-57. doi: 10.1021/acsbiomaterials.8b00051.
43. Shoaib M, Bahadur A, Iqbal S, Al-Anazy MM, Laref A, Tahir MA, et al. Magnesium doped mesoporous bioactive glass nanoparticles: a promising material for apatite formation and mitomycin c delivery to the MG-63 cancer cells. *J Alloys Compd* **2021**; 866: 159013. doi: 10.1016/j.jallcom.2021.159013.
44. Bibi A, ur-Rehman S, Akhtar T, Akhter K, Rafique S, Faiz R. Synthesis of alginate-based nanocomposites: a novel approach to antibacterial films. *Chem Zvesti* **2022**; 76: 3425-35. doi: 10.1007/s11696-022-02107-1.
45. He Z, Jiao C, Wu J, Gu J, Liang H, Shen L, et al. Zn-doped chitosan/alginate multilayer coatings on porous hydroxyapatite scaffold with osteogenic and antibacterial properties. *Int J Bioprint* **2023**; 9: 668. doi: 10.18063/ijb.v9i2.668.
46. Li Y, Liu X, Gaihre B, Li L, Rezaei A, Miller AL, et al. Zinc-doped hydroxyapatite and poly(propylene fumarate) nanocomposite scaffold for bone tissue engineering. *J Mater Sci* **2022**; 57: 5998-6012. doi: 10.1007/s10853-022-06966-7.